AR-009-678

DSTO-TR-0325

Numerical Simulation of Projectile Impact Experiments Using The Forest Fire Reaction Rate Model

Rodney A.J. Borg
and David A. Jones

DEPARTMENT OF DEFENCE
DEFENCE SCIENCE AND TECHNOLOGY ORGANISATION

DISCLAIMER NOTICE

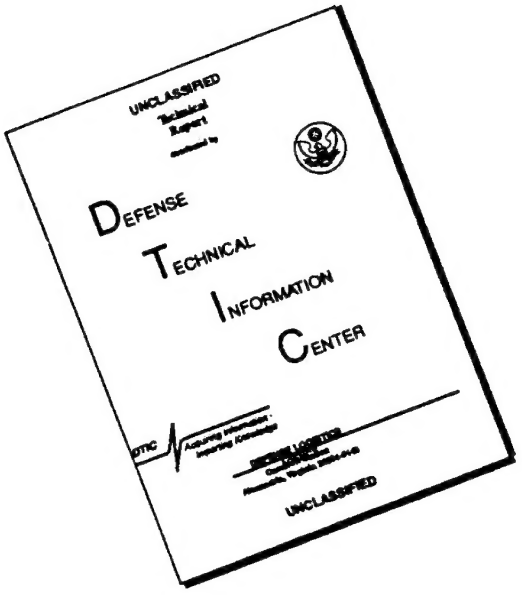

THIS DOCUMENT IS BEST QUALITY AVAILABLE. THE COPY FURNISHED TO DTIC CONTAINED A SIGNIFICANT NUMBER OF PAGES WHICH DO NOT REPRODUCE LEGIBLY.

Numerical Simulation Of Projectile Impact Experiments Using The Forest Fire Reaction Rate Model

Rodney A. J. Borg & David A. Jones

Weapons Systems Division
Aeronautical and Maritime Research Laboratory

DSTO-TR-0325

ABSTRACT

We describe the development of a two-dimensional multimaterial reactive Eulerian hydrocode to model the detonation of condensed phase explosives, and use the code to model the projectile impact initiation of explosives. The code solves the Euler equations for the conservation of mass, momentum, and energy for an inviscid, compressible fluid using the Flux Corrected Transport algorithm. The condensed phase materials are modelled using a Mie-Gruneisen equation of state, while the Becker-Kistiakowsky-Wilson equation of state is used to describe the gaseous detonation products. The Forest Fire reaction rate model is used to describe the rate of energy release from the explosive, and a modified Young's algorithm is used to maintain a sharp interface between different materials on the computational mesh. The code was used to simulate the impact of a cylindrical steel projectile against Composition B explosive, and the threshold velocity for the onset of detonation was found to be dependent on the diameter of the projectile. Our computed results are in good agreement with experimental values, as well as with results obtained from Mader's 2DE reactive hydrocode. The work described here will provide the ADF with an improved methodology to assess bullet/fragment hazards, and assist in the development of an Insensitive Munitions capability.

DEPARTMENT OF DEFENCE

DEFENCE SCIENCE AND TECHNOLOGY ORGANISATION

Published by

DSTO Aeronautical and Maritime Research Laboratory
PO Box 4331
Melbourne Victoria 3001

Telephone: (03) 9626 8111
Fax: (03) 9626 8999

AR No. AR-009-678
July 1996

APPROVED FOR PUBLIC RELEASE

Numerical Simulation Of Projectile Impact Experiments Using The Forest Fire Reaction Rate Model

Executive Summary

The Australian Defence Force Insensitive Munitions (IM) policy has rated bullet/fragment impact as one of the three major hazards to munitions in the Australian defence context. A key to reducing vulnerability is having the capability to predict the response of candidate munitions when subjected to designated hazards. The work reported here is concerned with understanding the processes and reactions which control the response of explosive fillings to various types of projectile impact. This will provide the ADF with an improved methodology to assess bullet/fragment hazards which can be applied to the assessment of existing munitions, and also facilitate the ADF "smart buyer" capability for IM items.

The report describes the development of a two-dimensional multimaterial Eulerian hydrocode to model the effects of projectile impact on condensed phase explosives, and the effects of the induced detonation on surrounding materials. An important part of the study was the use of the code to determine the threshold velocity separating detonation from non-detonative events. The code solves the Euler equations for the conservation of mass, momentum, and energy for an inviscid, compressible fluid. Operator splitting is used to reduce the complexity of the two-dimensional calculation, and the resulting one-dimensional equations are solved using the Flux Corrected Transport (FCT) algorithm of Boris and Book. This has fourth order phase accuracy, and an overall second order accuracy on uniform grids. A Mie-Gruneisen equation of state is used to describe the non-energetic condensed phase materials, while the Becker-Kistiakowsky-Wilson equation of state is used to describe the reacted explosive, and a modified Mie-Gruneisen equation of state is used to describe the unreacted explosive. The rate of energy release from the energetic material is described by the Forest Fire reaction rate model.

A modified Young's algorithm is used to maintain a sharp interface between different materials on the computational mesh. In this scheme an interface within a cell is approximated by a straight line. A computational cell containing more than one type of material uses information from each of its eight neighbouring cells to determine the exact points of intersection between the material interfaces and the cell walls. This removes the need for the specialised corner treatments which are needed when fully one-dimensional interface tracking algorithms are used.

We describe the application of the code to simulate the impact of a cylindrical steel projectile against the military explosive Composition B. At relatively high projectile velocities the impact produces a detonation of the explosive, while for lower velocities a less violent release of energy known as a deflagration occurs. The threshold velocity for the onset of detonation is dependent on the diameter of the projectile, and we have used the multimaterial code to determine threshold velocity as a function of projectile diameter. Our computed results are in good agreement with experimental values, as well as with results obtained from Mader's 2DE reactive hydrocode.

Authors

Rodney A.J. Borg
Weapons Systems Division

Rodney Borg graduated from the University of Melbourne with a B.Sc (Hons) in Chemistry in 1987. He joined the then MRL in 1988 and undertook a Ph.D. from Flinders University in Physical Chemistry in 1993. Since then he has worked on various experimental and theoretical projects with high explosives. He left AMRL in February 1996 to work with Kodak.

David A. Jones
Weapons Systems Division

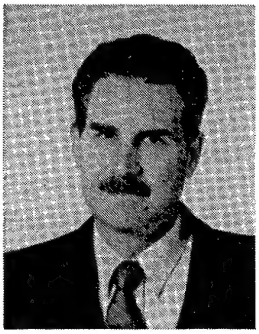

David Jones graduated from Monash University in 1972 with a BSc (Hons), and in 1976 with a PhD in Theorectical Physics. After working at Strathclyde University, London University and the Universtiy of New South Wales he joined AMRL in 1983 to work on the numerical and analytical modelling of shaped charge warheads. From February 1987 to May 1988 he was a Visiting Scientist at the Naval Research Laboratories in Washington DC. While there he worked on advanced computational fluid dynamics algorithms and their application to the numerical modelling of detonation and explosive effects.

Contents

1. Introduction

Weapons Systems Division is currently engaged in an experimental and numerical modelling program to study the response of explosive filled ordnance to projectile attack. The work is being conducted in response to the adoption of an Insensitive Munitions policy by the Australian Defence Force, and the identification of bullet/fragment impact as one of the three major hazards to munitions in the Australian defence context. The report by Swinton and Chick [1] describes the development of a projectile impact test designed to find the critical impact velocity for detonation of the target explosive, and its application to bullet impact experiments conducted on Australian manufactured Composition B explosive. The experiments use cylindrical copper projectiles, and these are fired against both bare and covered Composition B. Experiments have been conducted on Composition B made from boiled and milled RDX (which is the current filling used in Australian ordnance), as well as on Composition B made from recrystallised RDX, which is to replace the boiled and milled material when stocks run out. The experiments have shown that the Composition B made from recrystallised RDX is significantly less sensitive to projectile impact than that made from boiled and milled RDX, and one of the objectives of the experimental work is to investigate the controlling parameters and mechanisms of the initiation process.

This report describes the initial stages in the development and application of a two-dimensional (2D) multimaterial Eulerian hydrocode to model the response of explosive fillings to various types of projectile impact. Starkenberg et al. [2] have previously used the Los Alamos 2DE code to model projectile impact shock initiation of both bare and covered Composition B charges using cylindrical steel projectiles. They used the 2DE code to determine the critical impact velocity as a function of projectile diameter for bare explosive, and found that their results were in excellent agreement with the experimental results of Slade and Dewey [3], and the Jacobs-Roslund empirical formula [4].

The 2DE code is a reactive two-dimensional Eulerian hydrocode which uses the HOM equation of state to model both reacted and unreacted explosives, and the Forest Fire reaction rate model to describe explosive decomposition [5]. The AMRL code under development in WSD uses the same equations as the 2DE code to describe the explosive response, but the solution of the transport equations, and the treatment of material interfaces, use more advanced numerical techniques. The AMRL code uses the Flux Corrected Transport (FCT) algorithm to solve the Euler equations [6], and material interfaces are maintained using a Youngs interface tracking algorithm [7].

The experiments of Swinton and Chick have concentrated on the effect of RDX particle size on the critical velocity threshold. The Forest Fire reaction rate model was not designed to include particle size effects however, and so we have used the AMRL code, in its current state of development, to model the original experiments of Slade and Dewey.

In Section 2 we outline the development of the AMRL 2D Eulerian multimaterial hydrocode, and in Section 3 we use the code to model the projectile impact experiments of Slade and Dewey. In Section 4 we discuss some of the insights obtained from the simulations, and describe the further improvements which must be made to the code to model the projectile impact experiments of Swinton and Chick.

2. Description of Multimaterial Hydrocode

2.1 Basic Equations

Detonation phenomena occur on the microsecond time scale, and it is usual to assume that energy transport by heat conduction, viscosity, and radiation is negligibly small compared with transport by motion. The pressures generated by the detonation of a condensed phase explosive are of the order of 10^5 atmospheres. Under these conditions the strength of any confining material is completely negligible, and the material responds hydrodynamically. In this case, the appropriate equations which describe the material response are the Euler equations, which describe the conservation of mass, momentum and energy for an inviscid, compressible fluid. These have the following form [8]:

$$\frac{\partial \rho}{\partial t} + \nabla \cdot (\rho \mathbf{v}) = 0 \tag{1}$$

$$\frac{\partial (\rho v)}{\partial t} + \nabla \cdot (\rho \mathbf{v}\mathbf{v}) = -\nabla P \tag{2}$$

$$\frac{\partial E}{\partial t} + \nabla \cdot (E\mathbf{v}) = -\nabla \cdot (P\mathbf{v}) \tag{3}$$

In equations (1) - (3), ρ is the density, $\mathbf{v}$ the fluid velocity, P the hydrodynamic pressure, and E the total energy per unit volume, which is given by the following expression

$$E = \rho e + 0.5\rho v^2 \tag{4}$$

where e is the specific internal energy. The non-reactive materials are described by the Mie-Gruneisen equation of state, which has the form [9]:

$$P = P_H + \gamma(e - e_H)\rho \tag{5}$$

where P_H and e_H refer to the pressure and specific internal energy along the shock compression curve, known as the Hugoniot, and which have the form

$$P_H = P_0 + \rho_0 c_0^2 \eta/(1-s_0\eta)^2 \quad (6)$$

$$e_H = e_0 + 0.5(P_H + P_0)\eta/\rho_0 \quad (7)$$

where η is the compression, defined by $\eta = 1-\rho_0/\rho$, and c_0 is the sound speed in the undisturbed material. In the above expressions the shock velocity u_s and the particle velocity u_p are assumed to obey a linear relationship of the form

$$u_s = c_o + s_0 u_p.$$

The energetic materials require different equations of state to describe the condensed phase material before detonation, and the gaseous detonation products after reaction. The Mie-Gruneisen EOS is used to describe the unreacted material, while the BKW EOS is used to describe the highly non-ideal gaseous products after reaction. This has the form [10]:

$$P_g V_g/(RT) = 1 + x*\exp(\beta x) \quad (8)$$

where $x = k/[v_g(T+\theta)^\alpha]$ and k is the average covolume defined in terms of the individual covolumes k_i as $k = \kappa\sum x_i k_i$, where x_i is the mole fraction of species i. The α, β, κ, and θ are constants adjusted to reproduce the detonation pressure and velocity obtained experimentally.

The condensed explosive is converted into gaseous detonation products according to the Forest Fire reaction rate law [10],

$$\frac{d\lambda}{dt} = (1-\lambda)\exp\left(\sum_{i=0}^{i=14} a_i P^i\right) \quad (9)$$

where λ represents the fraction of reacted explosive. The finite rate of burning expressed by equation (9) yields a reaction zone of finite thickness in which λ varies between 0 and 1, and which contains a mixture of condensed explosive and gaseous products. In such regions we assume thermal and mechanical equilibrium between the two phases of the explosive and use an iterative technique to determine the specific internal energy of each phase.

2.2 Numerical Scheme

We have investigated two approaches to the solution of the coupled equations described above. In both cases operator splitting was used to decouple the transport stage from the chemical reaction stage, and then the two-dimensional transport equations were further decoupled into two sets of one-dimensional equations. This standard technique is described in detail in Oran and Boris [6].

In the first version of the code the density of each material on the grid was convected independently by making repeated calls to the LCPFCT algorithm [11] for each material. The momentum flux and total energy flux (ie. specific internal energy plus

kinetic energy) for each material were then added and the combined fluxes convected using LCPFCT. This approach is illustrated in the equations listed below, which show the sequence of equations to be solved for the x-pass in a 2D cartesian grid calculation; ρ_i is the density of the i'th material on the grid, ρu and ρv are the x and y components of the TOTAL momentum in each cell, and E is the TOTAL energy per unit volume in each cell.

$$\frac{\partial \rho_i}{\partial t} + \frac{\partial \rho_i u}{\partial x} = 0 \tag{10}$$

$$\frac{\partial \rho u}{\partial t} + \frac{\partial \rho u u}{\partial x} = -\frac{\partial P}{\partial x} \tag{11}$$

$$\frac{\partial \rho v}{\partial t} + \frac{\partial \rho v u}{\partial x} = 0 \tag{12}$$

$$\frac{\partial E}{\partial t} + \frac{\partial E u}{\partial x} = -\frac{\partial P u}{\partial x} \tag{13}$$

Because of the multimaterial capability of the code and the diffusive nature of all numerical transport schemes it is important to include an interface tracking algorithm to maintain a sharp interface between different materials on the grid. In the first version of the code we used the Simple Line Interface Calculation (SLIC) scheme of Noh and Woodward [12]. SLIC is a one-dimensional alternating direction method for the geometric approximation of fluid interfaces. The scheme constructs a representation of the interface between two materials from the volume fractions of the materials in the mixed cell, and by testing whether or not the various fluids in the mixed cell are present or absent in the zone just to the left and to the right in the coordinate direction under consideration. The interface between two different materials is therefore represented by a number of one-dimensional components, each of which is composed entirely of straight lines either perpendicular or parallel to the coordinate direction under consideration. LCPFCT assumes that the different materials in a mixed cell are spread homogeneously throughout the cell, and hence would calculate an incorrect flux in a mixed cell. The SLIC algorithm determines the correct amount of material to be advected into and out of a mixed cell, and then the LCPFCT algorithm is modified by imposing a multiplicative area factor at the correct cell boundary for each material. Further details of this procedure can be found in the report by Milne and Carnegie [13].

If LCPFCT and SLIC are applied to the Euler equations using the above scheme then problems are found to occur in the vicinity of the interface because the jump conditions (which imply continuity of particle velocity and pressure across the interface) are not enforced. The simplest constraint which can be applied, and is consistent with the split operator approach of FCT, is to ensure continuity of velocity across the interface. This constraint has been added by ensuring that the velocities either side of a mixed cell are equal, with the velocity ahead of the interface being set to that behind it.

A further problem with the above scheme is that the code requires a unique pressure to be determined for each mixed cell, and to do this requires knowing the density and specific internal energy of each material in the cell. Whilst the above scheme convects the density of each material independently, only the total energy in each cell is convected, and so a way of dividing the total internal energy in each cell between the component materials must be devised. To do this we assumed pressure equilibrium between the materials in the mixed cell (this is a common assumption in multimaterial Eulerian codes) and used an iterative procedure to determine the internal energy of each component.

The above scheme was used to simulate the one-dimensional impact of a 50 mm thick aluminium flyer plate with a velocity of 1.0 mm/μs hitting a 50 mm thick slab of non-reactive PBX-9404 explosive. The computational cell size was 1.0 mm, the time step was 0.04 μs, and the interface between the aluminium and PBX-9404 was initially located between cells 50 and 51. The pressure and particle velocity profiles after 8 μs are shown in Figure 1. These show a shock moving forward into the PBX-9404 and backwards into the aluminium flyer. Simple shock impedance calculations (Meyers, [9]) can be used to show that the pressure and particle velocity across the interface should have values of 0.048 Mbars and 0.70 mm/μs respectively, and Figure 1 shows that the simulation reproduces these values quite accurately. Figure 1a however shows that there is a slight perturbation to the velocity profile at the position of the interface (which is located partway through cell 56), and Figure 1b shows an even greater perturbation to the pressure profile. While the magnitude of this perturbation is relatively small (approximately 8% for the pressure), we envisage applications for the code where perturbations to the pressure amplitude of this size may lead to larger errors, especially when the code is used to study detonation phenomena.

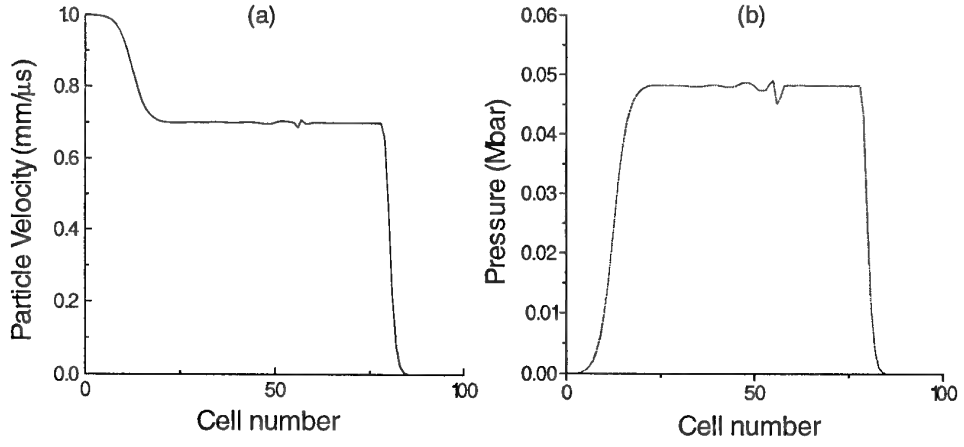

Figure 1. Simulated (using SLIC interface tracker) pressure and particle velocity profiles after 8 μs showing the one-dimensional impact of a 50 mm thick aluminium flyer plate with a velocity of 1.0 mm/μs hitting a 50 mm thick slab of non-reactive PBX-9404 explosive.

The source of these disturbances can be traced to the diffuse treatment of the total energy, and a discrepancy between the mass fluxes and interface velocities used in the partial density calculations and the momentum fluxes used in the principle momentum component equation. To improve the performance of the code it was decided to solve for the internal energy of each of the materials, and to replace the SLIC interface tracking algorithm with a scheme based on Youngs method [7]. The advantage of following the internal energy of each material is that an iterative calculation is no longer needed in each mixed cell, and the pressure in the cell is determined from a simple volume average of the partial pressures within the cell. The Youngs interface tracking scheme uses information from all eight of the mixed cells nearest neighbours, and hence provides a more accurate representation of the interface than the SLIC scheme. Additional changes to the code included a change in the way the principal component of the momentum was calculated. In the new scheme the momentum is calculated by using the sum of the products of the mass fluxes calculated during the solution of the partial density equations, and the cell interface velocities, also used for the density calculations, thus ensuring consistency in terms of mass and velocity at the cell boundary. The sequence of equations to be solved for the x-pass in a 2D cartesian grid calculation now has the form shown below, where ρ_i and e_i are the density and specific internal energy respectively of the i'th material on the grid, and u and v are the x and y components of the velocity in each cell. This approach removes the need to enforce continuity of particle velocity across the interface. A detailed description of the new scheme can be found in the report by Carnegie [14].

$$\frac{\partial \rho_i}{\partial t} + \frac{\partial \rho_i u}{\partial x} = 0 \tag{14}$$

$$\frac{\partial u}{\partial t} + \frac{\partial uu}{\partial x} = u\frac{\partial u}{\partial x} - \frac{\nabla P}{\rho} \tag{15}$$

$$\frac{\partial v}{\partial t} + \frac{\partial vu}{\partial x} = v\frac{\partial u}{\partial x} \tag{16}$$

$$\frac{\partial e_i}{\partial t} + \frac{\partial e_i u}{\partial x} = -P\frac{\partial u}{\partial x} \tag{17}$$

The effect of these changes can be seen in Figure 2, which shows pressure and particle velocity profiles for the same 1D simulation of a 50 mm thick aluminium flyer plate with a velocity of 1.0 mm/μs hitting a 50 mm thick slab of non-reactive PBX-9404 explosive. The new scheme has calculated the general features of the flow quite accurately, although there are differences between the two schemes. Figure 2 shows that both the particle velocity and pressure are continuous across the interface and do not display the sharp discontinuities shown in Figure 1. This is quite a pleasing result, given that the new scheme neither imposes a velocity constraint across the interface, nor requires an iteration of the internal energy for the materials in a mixed cell to insure pressure equilibrium between the materials. Figure 2 also shows that the new scheme provides a better representation of the shock in the aluminium flyer. The

particle velocity plot in Figure 2a shows a sharper shock profile, as does the pressure profile in Figure 2b, although there is a slight perturbation to the pressure at the location of the front.

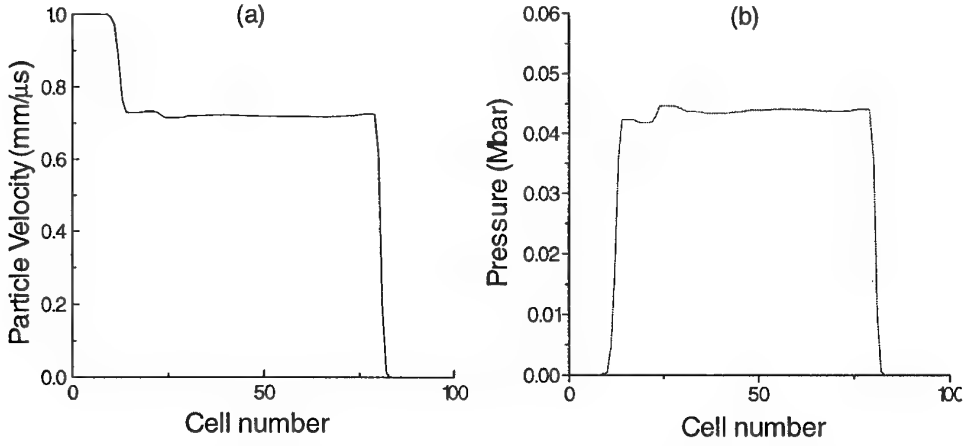

Figure 2. Simulated (using Youngs interface tracker) pressure and particle velocity profiles after 8 μs showing the one-dimensional impact of a 50 mm thick aluminium flyer plate with a velocity of 1.0 mm/μs hitting a 50 mm thick slab of non-reactive PBX-9404 explosive.

We have also repeated this simulation using a steel flyer plate impacting non-reactive Composition B. A 50 mm thick steel flyer plate travelling at 1.0 mm/μs impacted a 50 mm thick slab of unreactive Composition B explosive. The length of the computational cell was 1.0 mm, the time step was calculated from the Courant condition (approximately 0.1 μs), and the interface was initially located between cells 50 and 51. The results of the calculation after 8 μs are shown in Figure 3. One-dimensional shock impedance calculations predict that the pressure and particle velocity across the interface should be 0.057 Mbars and 0.853 mm/μs respectively. Figure 3 shows that the simulated particle velocity is approximately 0.84 mm/μs, while the simulated pressure is approximately 0.057 Mbars. These results are in good agreement with the 1D shock impedance calculations; the particle velocity is accurate to 1%, while the simulated pressure is no more than 5% too high. Figure 3 also shows that both particle velocity and pressure are continuous across the interface. Comparison of Figure 3 with Figure 2 however shows a slightly greater perturbation to the shock profiles for the steel impact problem, particularly for the pressure profile. This is caused by the greater difference in density between the two impacting materials for the steel/Composition B case than for the aluminium/PBX-9404 calculation. These perturbations are not fundamental however, and experimentation has shown that they can be reduced by using a finer time step during the first few microseconds of the impact.

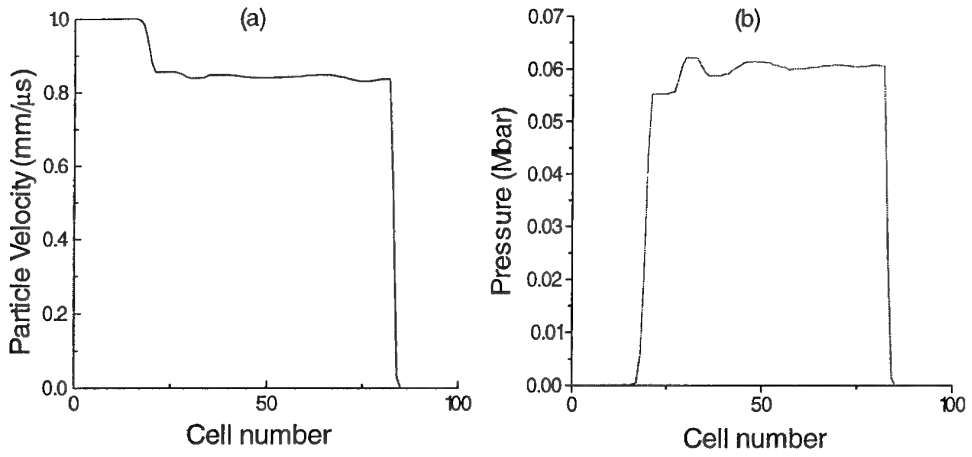

Figure 3. Simulated (using Youngs interface tracker) pressure and particle velocity profiles after 8 μs showing the one-dimensional impact of a 50 mm thick steel flyer plate with a velocity of 1.0 mm/μs hitting a 50 mm thick slab of non-reactive Composition B explosive.

3. Application to Projectile Impact Experiments

Since the Forest Fire reaction rate model is unable to model particle size effects, and therefore cannot be used to simulate the Swinton and Chick results, it was decided to test the capabilities of the code in its present stage of development by modelling the earlier projectile impact experiments of Slade and Dewey. These experiments used steel cylinders of varying diameters fired against Composition B to determine the critical impact velocity for initiation as a function of the projectile diameter. The experiments were later modelled by Starkenberg et al. using the 2DE code, and good agreement was found between the calculations and the experimental results. Considering that the equations of state and reaction rate law for Composition B used in our current version of the AMRL code are the same as those used by Starkenberg et al., we would expect that simulations of projectile impact using our code should be in good agreement with the results found by the above authors.

3.1 Geometry and Computational Considerations

The projectile impact calculations were performed using 2D cylindrical geometry. The basic grid is illustrated in Figure 4. This shows the cylindrical steel projectile, the cylindrical Composition B explosive charge, and the surrounding air. In all the simulations the projectile was initially just in contact with the explosive and had a positive initial velocity, indicating that the direction of motion was towards the explosive. The initial pressure of the air, projectile and high explosive was one atmosphere (ie. 101325Pa), and this determines the state of the respective materials via the appropriate equation of state.

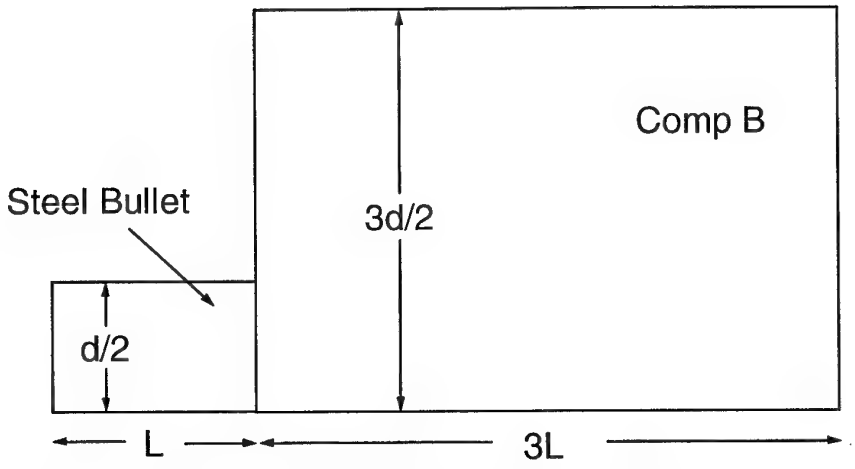

Figure 4. Schematic illustration of the 2D cylindrical geometry used in the calculations showing the cylindrical steel projectile, the cylindrical Composition B explosive charge, and the surrounding air.

3.2 Steel projectile / Bare Composition B impact results

The critical velocity (V_c) is defined as the velocity of the projectile above which projectile impact results in shock initiation, and below which the impact results in a lower order event such as a burn or deflagration. Experimentally it has been found that the critical velocity increases as the diameter of the projectile is reduced. In the calculations reported here the speed of the projectile has been varied to determine the critical velocity for each projectile diameter. In this process, it is important to carefully determine the type of event caused by the projectile impact. Starkenberg et al. [2] used contours of the explosive mass fraction to determine the outcome of projectile impact simulations, with detonation being recognised by the close spacing of the contour lines. In this context, mass fraction refers to the amount of unreacted explosive, thus a mass fraction of 1 corresponds to wholly unreacted explosive, and a mass fraction of zero represents complete reaction of the explosive. In this work, colour contour plots of the pressure and the speed of the reaction front are also used to determine the outcome of the projectile impact calculation.

Figure 5 shows the results from the impact of a 6.75 mm diameter steel projectile on bare Composition B. In this example the projectile velocity is 1.24 mm/μs and the impact results in a detonation. This is evident from the close spacing of the black contour lines of the explosive mass fraction, and by the high pressure at the shock front shown by the colour pressure contours (red represents the highest pressure). Figure 6 shows contour plots from an identical run, except with a projectile velocity of 1.12 mm/μs, and this clearly shows a failure. In this case the black contour lines of the explosive mass fraction are widely spaced and the pressure at the shock front is relatively low.

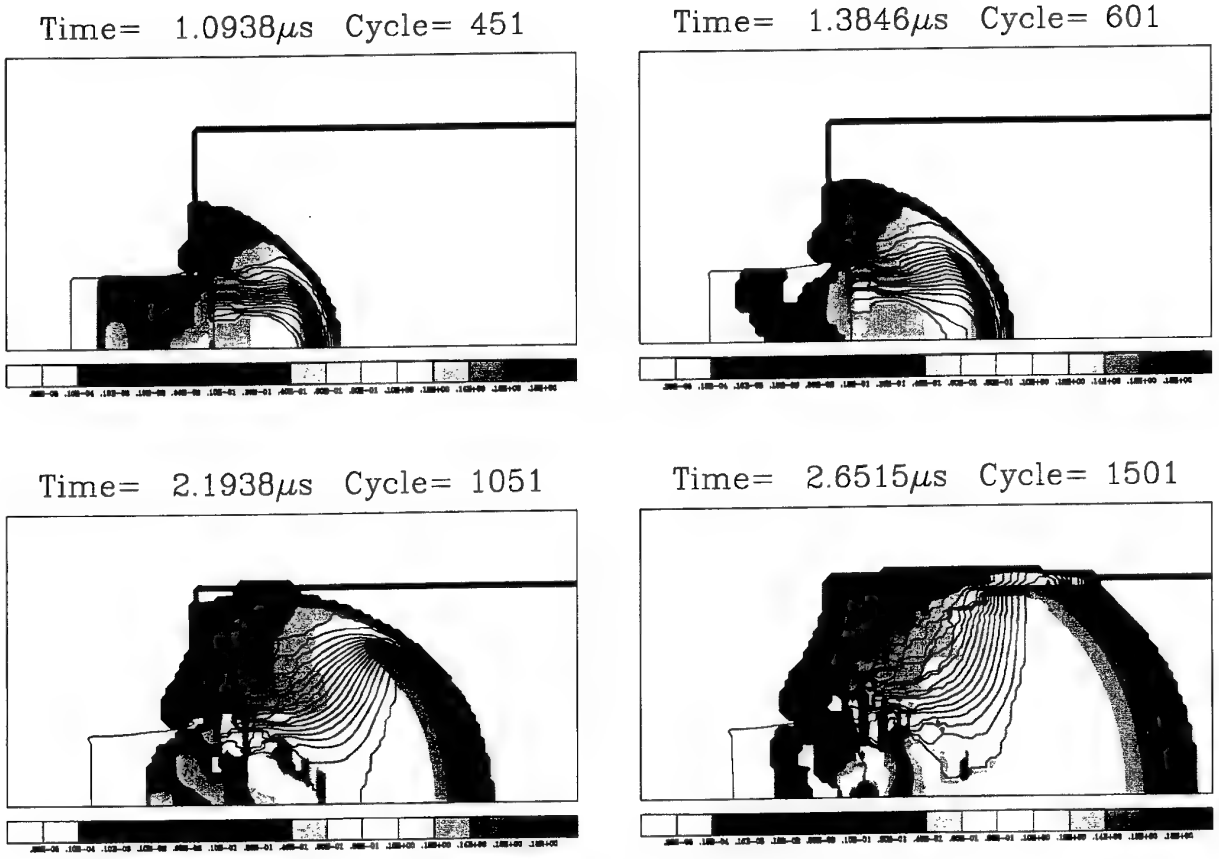

Figure 5. Simulated results from the impact of a 6.75 mm diameter steel projectile travelling at 1.24 mm/ms on bare Composition B.

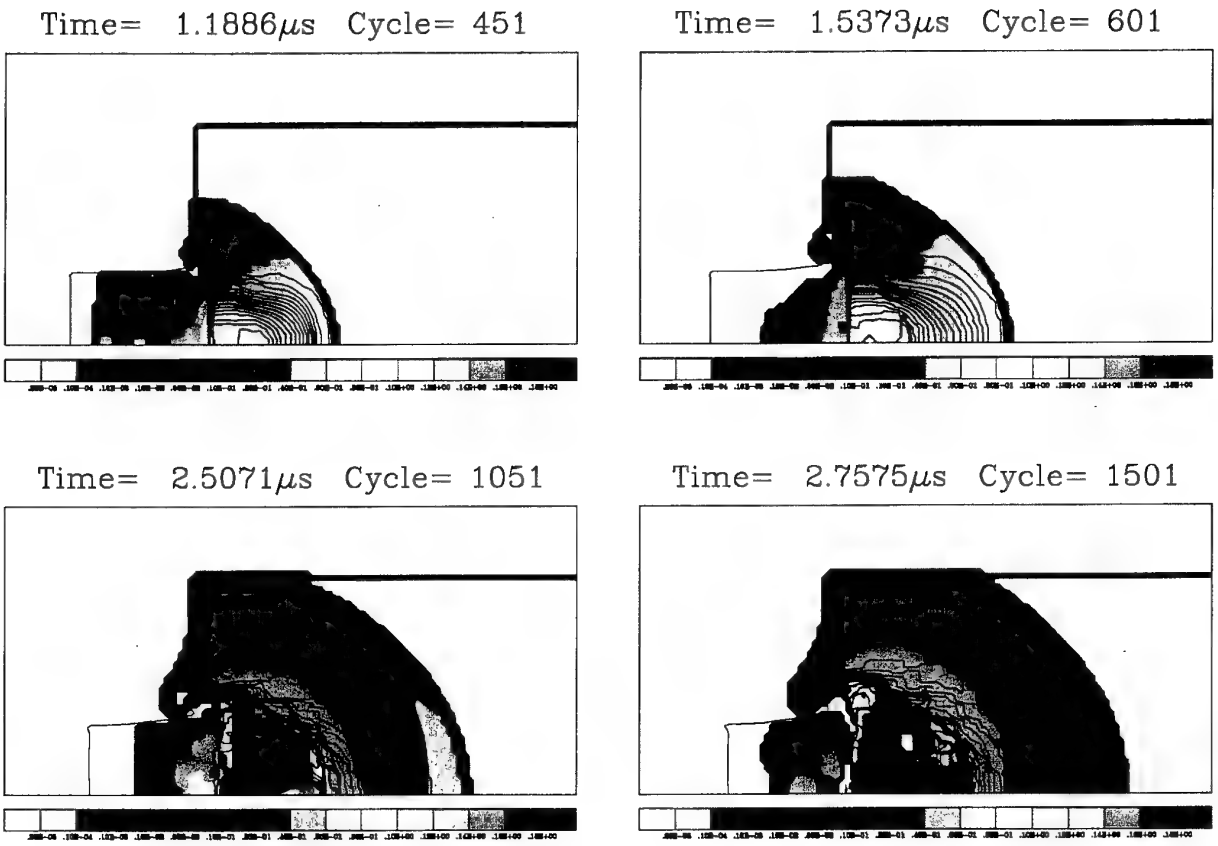

Figure 6: Simulated results from the impact of a 6.75 mm diameter steel projectile travelling at 1.12 mm/μs on bare Composition B.

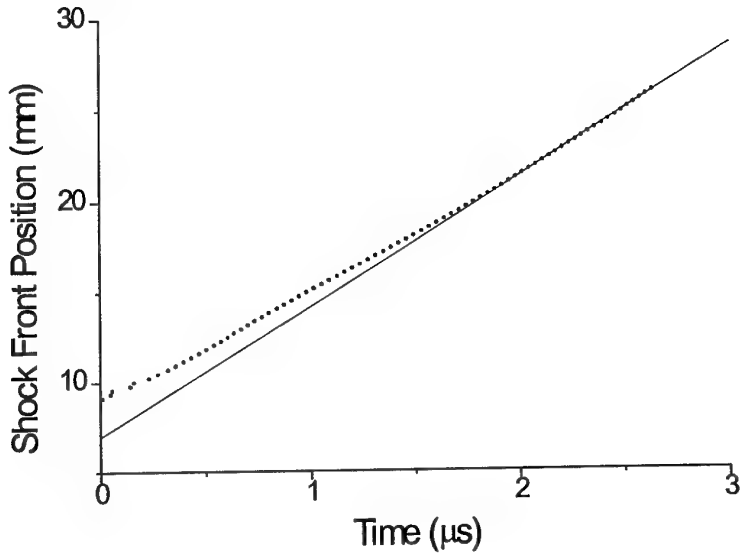

Figure 7. Plot of shock front position as a function of time for the 6.75 mm projectile impacting the bare explosive at 1.24 mm/μs. The dots denote the computed position, while the solid line is a line of best fit calculated from the last third of the points, indicating that the speed of the shock front increases towards the end of the run.

The velocity of the impact shock front also gives an indication of the type of outcome produced by the projectile impact. The plot of shock front position as a function of time for the 6.75 mm projectile impacting the bare explosive at 1.24 mm/μs is shown in figure 7. The slope of this plot represents the speed of the shock front and shows that as reaction proceeds the speed of the shock front increases and reaches a value of about 7.1 mm/μs. On the other hand, the corresponding plot for the 6.75 mm projectile travelling at 1.12 mm/μs, shown in Figure 8, exhibits the reverse behaviour. In this case the velocity of the shock front decreases and the final velocity is approximately 4.2 mm/μs. Although the detonation velocity of Composition B is 8.0 mm/μs, the value of 7.1 mm/μs is not the final, steady-state velocity. If the calculation was allowed to proceed further, the reaction front velocity would increase towards the expected value. Nonetheless, plots of shock front position as a function of time help to determine the outcome of the projectile impact. If the shock front velocity increases with time, the reaction is accelerating and this indicates a detonation, whereas a decelerating shock front is indicative of a failure.

Table 1 summarises the important parameters of the computations performed in our study of steel projectile impact on bare Composition B. In this table, d is the projectile diameter, dx and dy are the grid sizes in the x and y directions, ncx and ncy are the number of cells in the x and y directions, Cycles is the number of time steps performed in the simulation, and Elapsed Time is the cumulative total of dt, the time step, at the end of the run. The outcome of the particular projectile impact is deduced by examining the mass fraction contours, colour contour plots of the pressure profiles, and plots of the shock front position as a function of time.

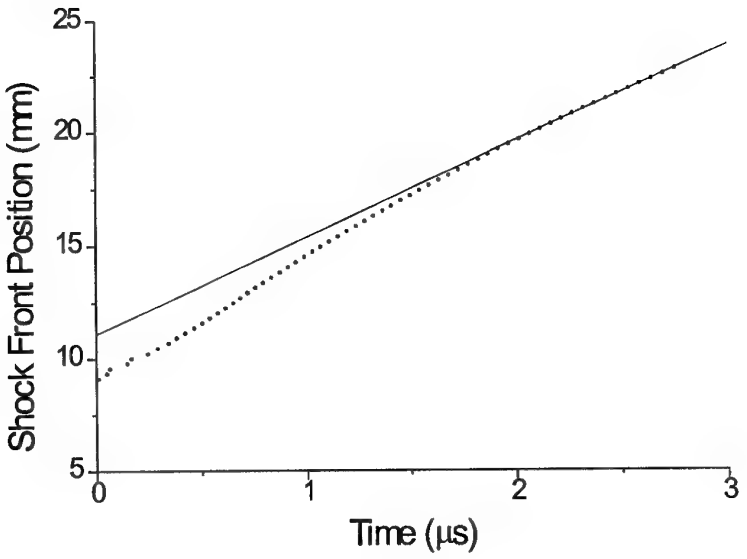

Figure 8. Plot of shock front position as a function of time for the 6.75 mm projectile impacting the bare explosive at 1.12 mm/μs. The dots denote the computed position, while the solid line is a line of best fit calculated from the last third of the points, indicating that the speed of the shock front decreases towards the end of the run.

The critical velocity is known to be an inverse function of the projectile diameter, ie., $V_c = kd^{-n}$. Starkenberg et al. have used n = 0.5 to plot their results on the projectile impact of Composition B, but n = 1 appears to give a better fit to the experimental data, as demonstrated by Liddiard and Rosland [15]. Hence in this report we use n = 1 when comparing our results with previously published work.

Figure 9 shows a plot of V_c versus 1/d for our results, the experimental results of Slade and Dewey [3], and the 2DE computations of Starkenberg et al. [2]. The 2DE code uses the HOM EOS and the Forest Fire reaction rate model to describe the explosive response, but the treatment of both the material transport and material interfaces is entirely different from the methods described here. 2DE uses a finite difference scheme based on the work of Gentry et al. [19] to solve the transport equations. This is a low order scheme which relies on the use of an artificial viscosity to stabilize the shock, and hence is less accurate than the FCT scheme employed here. The treatment of mixed cells in 2DE is based on the donor-acceptor method developed by Johnson [20]. This has limited resolution, and is unable to locate the position of the interface within the mixed cell. The Youngs interface tracking algorithm used in the present code has greater resolution, and is able to draw an accurate representation of the interface within each cell.

Table 1: Steel projectile impact on bare Composition B - summary of runs.

d (mm)	dx/dy (mm)	ncx	ncy	Cycles	Elapsed Time (μs)	Projectile velocity (mm/μs)	Outcome
4.0	0.133	200	60	4500	2.481	1.66	Fail
4.0	0.133	300	60	6000	3.120	1.68	Det.
5.0	0.167	200	60	4500	2.929	1.38	Fail
5.0	0.167	200	60	6000	3.037	1.40	Det.
6.75	0.225	160	60	3000	4.450	1.14	Fail
6.75	0.225	160	60	3000	3.981	1.16	Det.
8.0	0.267	120	60	1500	3.299	1.04	Fail
8.0	0.267	120	60	1500	3.458	1.06	Det.
10.0	0.333	200	60	3000	4.575	0.92	Fail
10.0	0.333	120	60	1500	4.685	0.94	Det.
12.0	0.4	200	60	3000	6.948	0.82	Fail
12.0	0.4	200	60	3000	6.925	0.84	Det
15.0	0.5	200	60	3000	7.007	0.72	Fail
15.0	0.5	120	60	1500	6.939	0.76	Det.
18.0	0.6	300	60	1500	7.955	0.67	Fail
18.0	0.6	300	60	1500	8.124	0.68	Det.

Our calculated results are in close agreement with the calculations of Starkenberg et al., although there appears to be a consistent discrepancy at larger projectile diameters, where the Starkenberg et al. results indicate a slightly lower critical velocity in comparison to our results. The magnitude of the difference is not great however, and we believe this may be attributed to the different methods used to distinguish between detonation and failure by the various authors, rather than to the differences between our code and the 2DE code. It should be noted that in our work the difference in the velocity of the projectile that produces a fail and a detonation is typically 0.02 mm/μs. Starkenberg et al. do not specify the change in projectile velocity between a fail and a detonation. The discrepancy between either of the computed critical velocities and the experimental results is larger than the difference between the two sets of computed values. The calculated results consistently predict a lower critical velocity than the experimental results. This can be attributed to deficiencies in the reaction rate model, Forest Fire, used for the explosive.

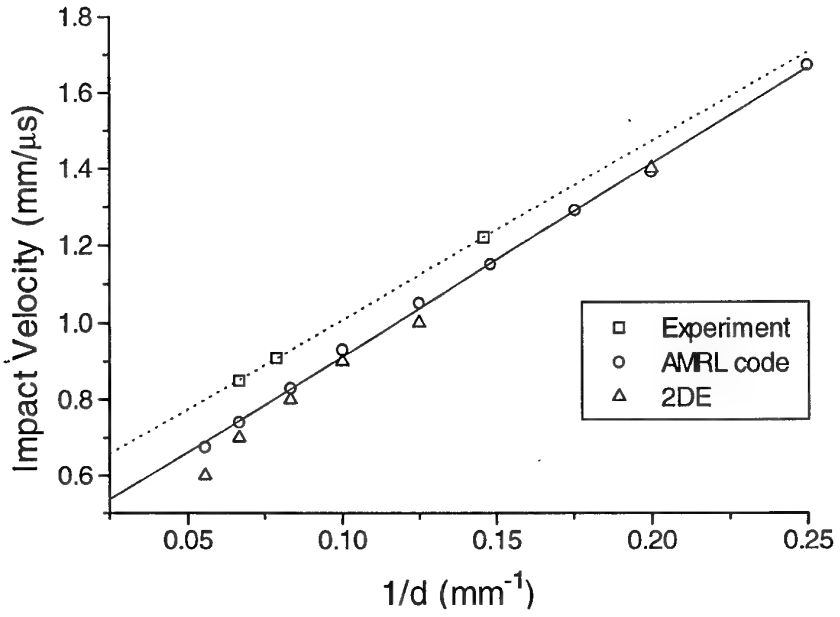

Figure 9. Plot of V_c versus 1/d for our results, the experimental results of Slade and Dewey, and the 2DE computations of Starkenberg et al.

4. Discussion and Conclusion

The simulation results shown in Figures 5 and 6 are examples of either a clear failure, or a clear detonation. However, during the course of the calculations it became apparent that the result was not always immediately clear, and it became necessary to perform longer runs to clarify the outcome. Figure 10 shows another example where a clear failure is immediately apparent. In this case the projectile had a diameter of 12.0 mm and an impact velocity of 0.76 mm/μs. In each of the four plots the pressure levels remain low and the mass fraction contour lines always remain well spaced, and none of the plots show any indication that a detonation will develop. The sequence shown in Figure 11 also represents a failure, however in this case it initially looks like a detonation. The projectile had a diameter of 4.0 mm, and an impact velocity of 1.60 mm/μs. At 0.3203 μs there is a region of high pressure just behind the reaction front and the mass fraction contour lines are closely spaced, but at 0.9295 μs the mass fraction contour lines have spread out indicating that the reaction is slowing down. By 1.8336 μs the contour lines become even further spaced and the pressure has reduced significantly, as indicated by the colour contours. This type of behaviour, where the detonation dies away, is observed for the smaller diameter projectiles.

In other cases the initial stages may look like a failure, but ultimately a detonation results. Such a sequence is shown in Figure 12, where the diameter of the projectile is

12.00 mm and the impact velocity is 0.84 mm/μs. At 4.4090 μs the mass fraction contour lines are widely spaced and the colour contours indicate relatively low pressures. However, by 6.0114 μs a strong reaction front has developed with closely spaced mass fraction contour lines and high pressure behind the front. This buildup continues and by 6.5665 μs a detonation has clearly formed.

An example of a prompt detonation sequence is shown in Figure 13. In this case the projectile diameter was 18.0 mm and the impact velocity was 0.82 mm/μs. High pressures and closely spaced mass fraction contour lines are apparent soon after the projectile impact. After this immediate initiation, the detonation continues to propagate. This type of prompt initiation is typical for the larger diameter projectiles.

The results presented above have shown the capabilities of the code in its present state of development, and our ability to accurately predict the critical velocity for projectile impact on Composition B when the Forest Fire coefficients appropriate to the particular composition under study are used. It is impractical however to develop the correct Forest Fire coefficients for each of the compositions studied by Swinton and Chick, and so an alternative procedure will have to be developed to model these results. Because the experiments show such a strong dependence on RDX particle size and/or morphology, any reaction rate scheme used to model the results will have to include an explicit dependence on particle size. Appropriate reaction rate schemes currently do not exist; however, by combining the Lee and Tarver Ignition and Growth reaction rate model [16] with the work of Kim [17] on particle size dependent reaction rates in shocked explosives, and the work of Murphy et al. on Composition B shock initiation [18], we anticipate that some insight into the experimental results might be obtained. Such work is proceeding.

5. Acknowledgments

We are grateful to Alec Milne and William Carnegie of Fluid Gravity Engineering Ltd. for numerous very helpful discussions concerning the numerical schemes used in this work.

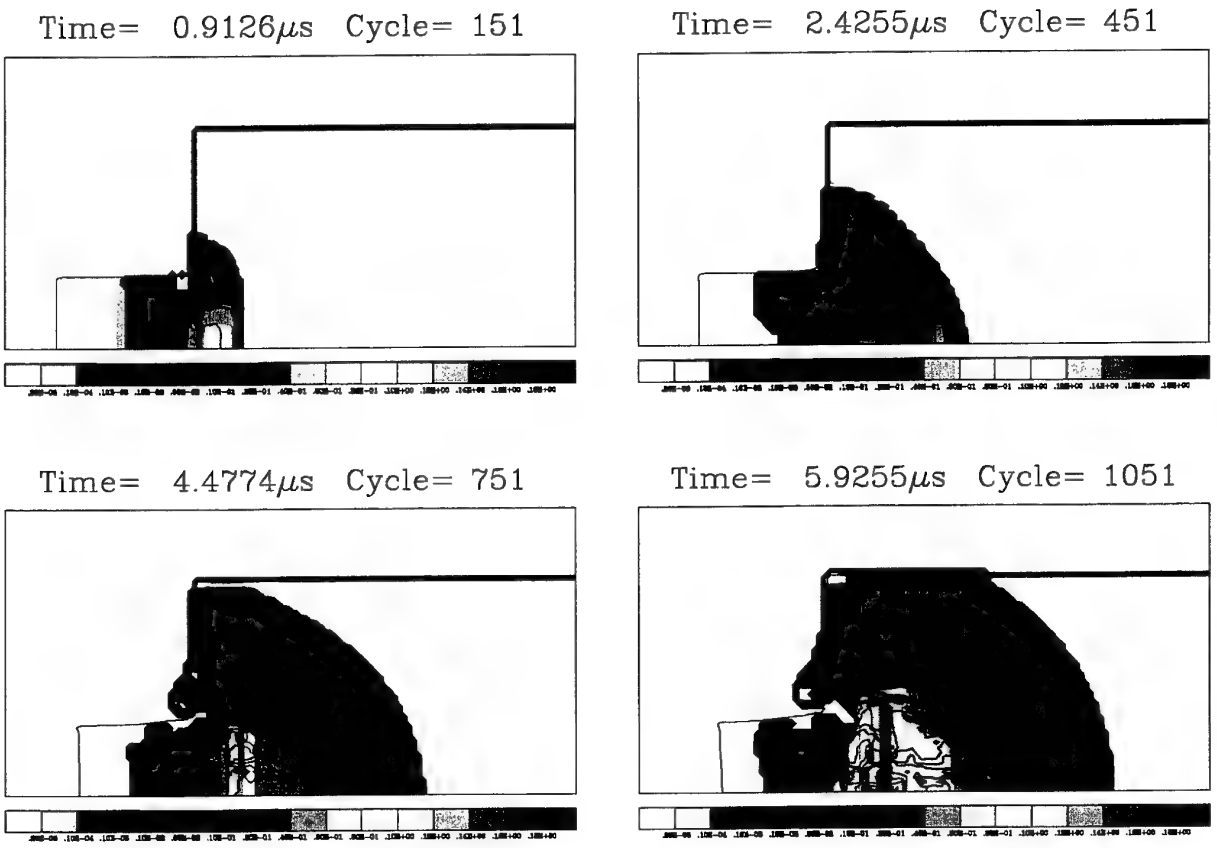

Figure 10: Simulated results from the impact of a 12.0 mm diameter steel projectile travelling at 0.76 mm/μs on bare Composition B. (clear failure is immediately apparent)

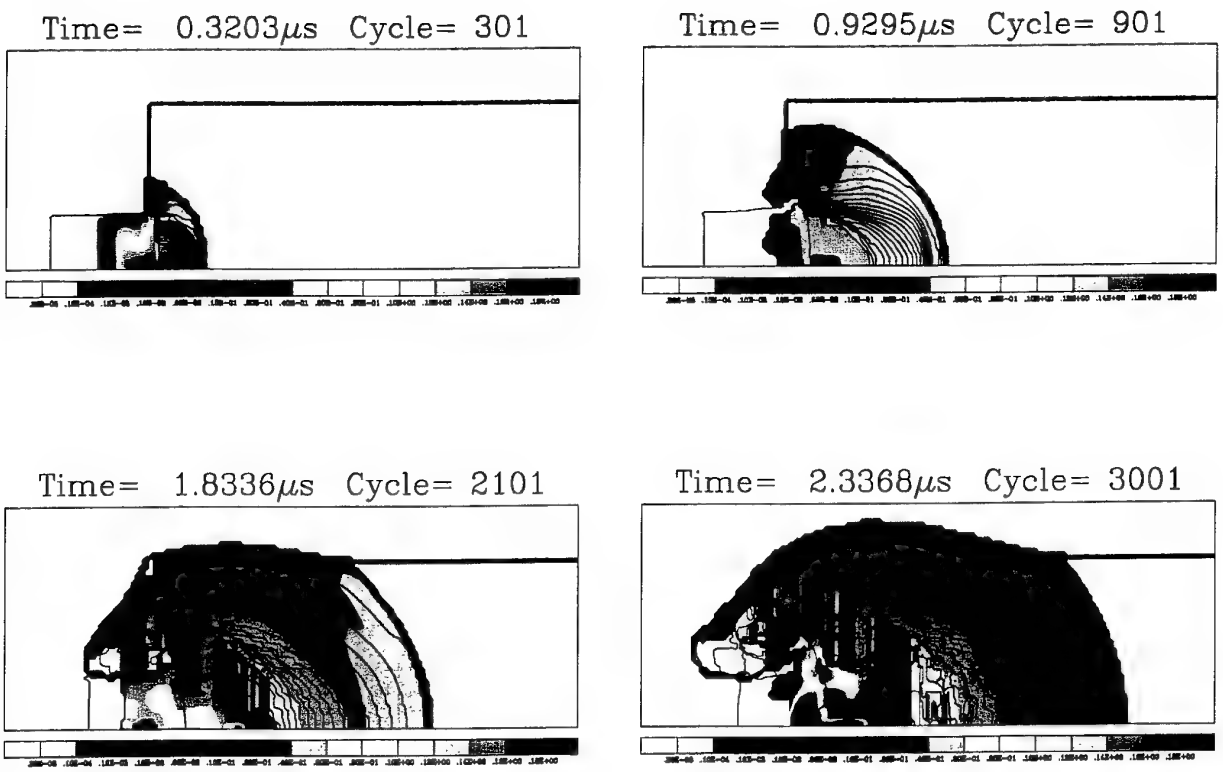

Figure 11: Simulated results from the impact of a 4.0 mm diameter steel projectile travelling at 1.60 mm/μs on bare Composition B.

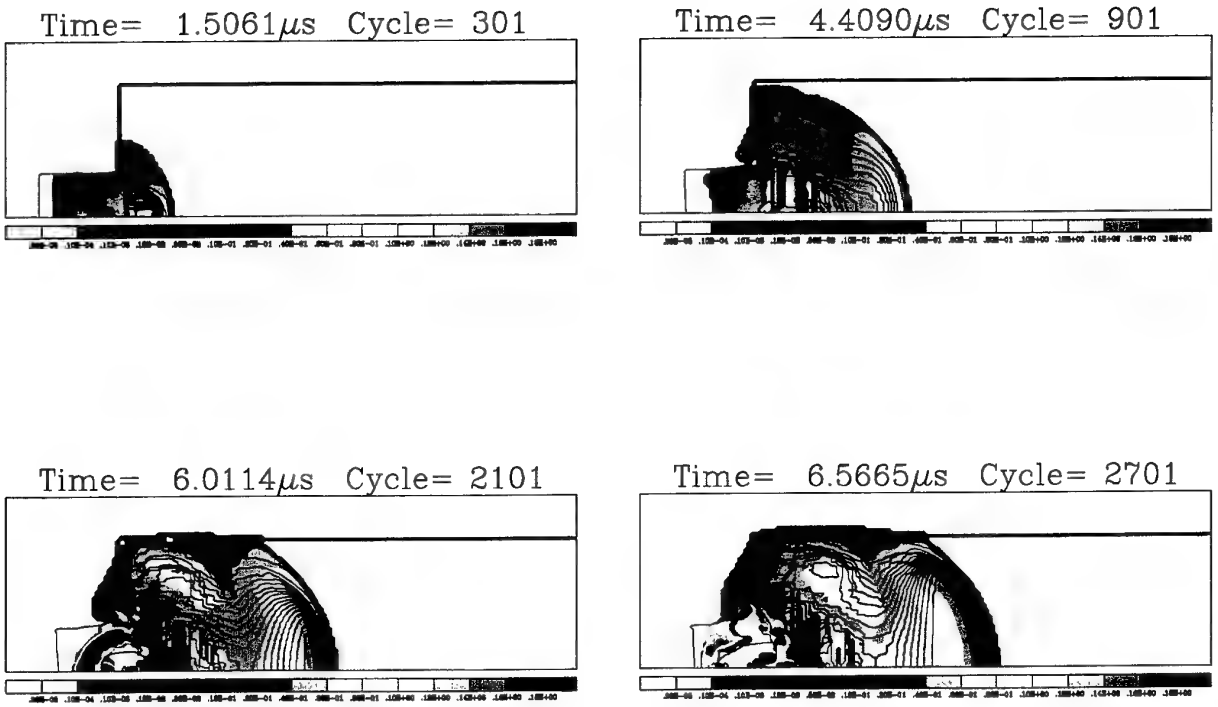

Figure 12: Simulated results from the impact of a 12.0 mm diameter steel projectile travelling at 0.84 mm/μs on bare Composition B. (initially looks like a fail, but ultimately a detonation results).

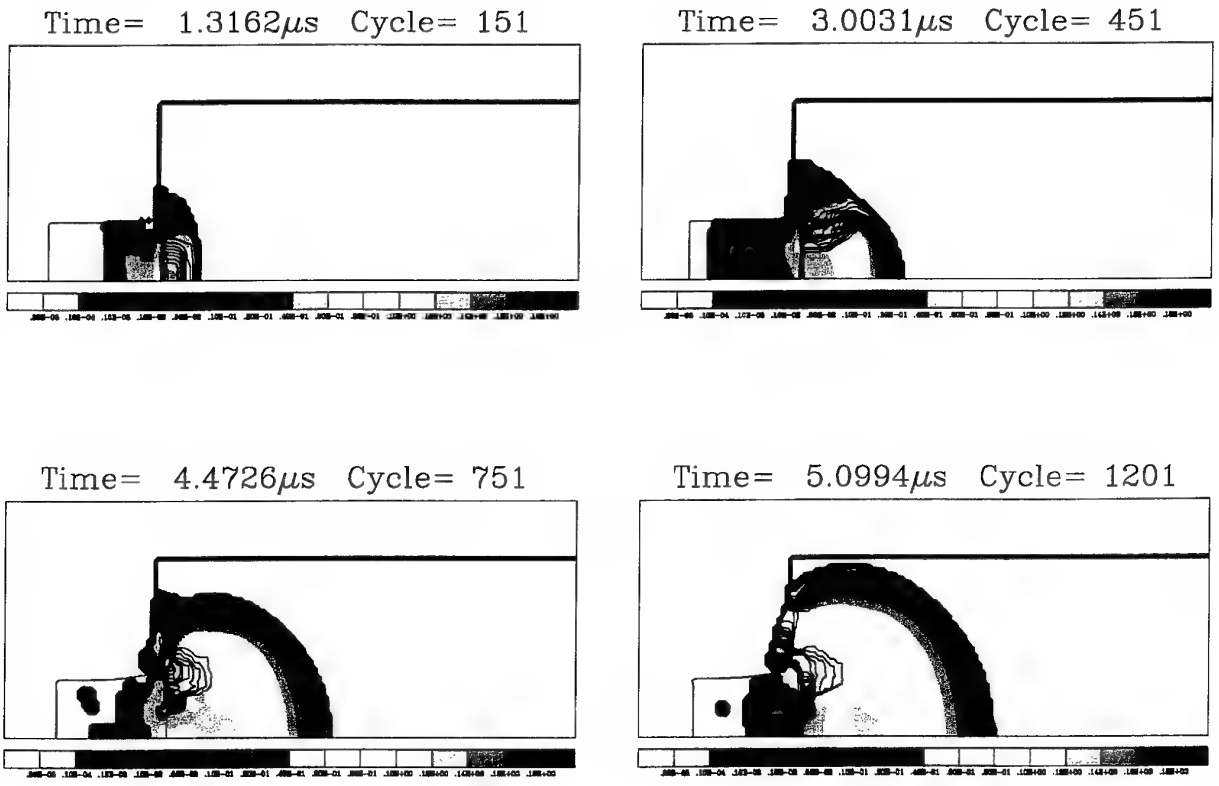

Figure 13: Simulated results from the impact of a 18.0 mm diameter steel projectile travelling at 0.82 mm/μs on bare Composition B. (example of a prompt detonation sequence).

6. References

1. Swinton, R.J. and Chick, M.C., *Projectile Impact of Australian Composition B*, DSTO Technical Report, in preparation.
2. Starkenberg, J., Huang Y. and Arbuckle A., *Numerical Modelling of Projectile Impact Shock Initiation of Bare and Covered Composition B*, Journal of Energetic Materials, **2**, Number 1-2, pp 1-42.
3. Slade, D.C. and Dewey, J., *High-Order Initiation of two Military Explosives by Projectile Impact*, Ballistics Research Laboratory Report No. 1021, July 1957.
4. Rosland L.A., Watt, J.W. and Cleburn, N.L., *Initiation of Warhead Explosives by the Impact of Controlled Fragments. 1 Normal Impact*, Naval Ordnance Laboratory Technical Report NOLTR-73-124, August 1974.
5. Kershner, J.D. and Mader, C.L. (1972) *2DE, A Two-Dimensional Continuous Eulerian Hydrodynamic Code for Computing Multicomponent Reactive Hydrodynamic Problems*, Los Alamos Scientific Laboratory Report LA-4846.
6. Oran, E.S. and Boris J.P., *Numerical Simulation of Reactive Flow*, Elsevier Science Publishing Co., Inc., New York, 1987.
7. Youngs, D.L., *Time Dependent Multi-Material Flow with Large Fluid Distortion, Numerical Methods for Fluid Dynamics*, K.W. Morton and M.J. Baines (eds.), 1982.
8. Cheret, R. (1993) *Detonation of Condensed Explosives*, Springer-Verlag, New York Inc.
9. Meyers, M.A. (1994) *Dynamic Behaviour of Materials*, John Wiley and Sons, Inc.
10. Mader, C.L., *Numerical Modelling of Detonations*, University of California Press, Berkeley, 1979.
11. Boris, J.P., Landsberg, A.M, Oran E.S. and Gardner, J.H., (1993) *LCPFCT - a flux corrected transport algorithm for solving generalized continuity equations*. NRL memorandum report 6410-93-7192, Washington, DC.
12. Noh, W.F and Woodward, P. (1976) *The SLIC (Simple Line Interface Calculation) Method*, UCRL-52111.
13. Milne, A.M. and Carnegie, W.D. (1993) *Implementation of a Simple Line Interface Calculation (SLIC) Scheme for use with LCPFCT*, Fluid Gravity Engineering Ltd. Report CR 102/93.
14. Carnegie, W.D. (1994) *An Improved SLIC Scheme for LCPFCT, Incorporating Multi-Material Thermodynamics*, Fluid Gravity Engineering Ltd., Report CR 102/94.
15. Liddiard, T.P. and Roslund, L.A. (1993) Projectile/Fragment Impact Sensitivity of Explosives, Naval Surface Warfare Centre, NSWC TR-89-184.
16. Lee, E.L. and Tarver, C.M., *Phenomenological model of shock initiation in heterogeneous explosives*, Phys. Fluids **23** (12), 2362 - 2372 (1980).
17. Kim, K. *Particle Size Dependent Reaction Rate in Shocked Explosives*, Shock Waves in Condensed Matter 1987, S.C. Schmidt and N.C. Holmes (editors), 531 - 534, Elsevier Science Publishers B.V., 1988.

18. Murphy, M.J., Lee, E.L., Weston, A.M. and Williams, A.E., *Composition B Shock Initiation Report*, Lawrence Livermore National Laboratory, UCRL-1D-118300, 1994.

19. Gentry, R.A. Martin, R.E. and Daly, B.J., *An Eulerian Differencing Method for Unsteady Compressible Flow Problems*, J. Comp. Phys, **1**, 87-118, 1966.

20. Johnson, W.E., *Development and Application of Computer Programs Related to Hypervelocity Impact*, Sysytems, Science and Software, SSS-R-353, 1970.

DISTRIBUTION LIST

Numerical Simulation Of Projectile Impact Experiments Using The Forest Fire Reaction Rate Model

Rodney A. J. Borg & David A. Jones

AUSTRALIA

TASK SPONSOR:

DEFENCE ORGANISATION

Defence Science and Technology Organisation

Chief Defence Scientist
FAS Science Policy
AS Science and External Relations
AS Science Corporate Management
} shared copy

Counsellor Defence Science, London (Doc Data Sheet only)
Counsellor Defence Science, Washington
Scientific Adviser to MRD Thailand (Doc Data Sheet only)
Senior Defence Scientific Adviser/ScientificAdviser Policy and Command (shared copy)
Navy Scientific Adviser
Scientific Adviser - Army
Air Force Scientific Adviser
Director Trials

Aeronautical and Maritime Research Laboratory

Director
Chief, Weapons Systems Division
Dr. R.J. Spear
M.C. Chick
Rodney A. J. Borg
David A. Jones

DSTO Library

Library Fishermens Bend
Library Maribyrnong
Main Library DSTOS (2 copies)
Library, MOD, Pyrmont (Doc Data sheet only)

Defence Central

OIC TRS, Defence Central Library
Officer in Charge, Document Exchange Centre (DEC), 1 copy
DEC requires the following copies of public release reports to meet exchange agreements under their management:
*US Defence Technical Information Centre, 2 copies
*UK Defence Research Information Centre, 2 copies
*Canada Defence Scientific Information Service, 1 copy
*NZ Defence Information Centre, 1 copy
National Library of Australia, 1 copy
Defence Intelligence Organisation
Library, Defence Signals Directorate (Doc Data Sheet only)

Army

Director General Force Development (Land),
ABCA Office, G-1-34, Russell Offices, Canberra (4 copies)
SO (Science), HQ 1 Division, Milpo, Enoggera, Qld 4057 (Doc Data Sheet only of Army sponsored reports)
NAPOC QWG Engineer NBCD c/- DENGRS-A, HQ Engineer Centre Liverpool Military Area, NSW 2174 (Doc Data Sheet only of Army sponsored reports)

Navy

Director General Force Development (Air), (Doc Data Sheet only)
Director General Force Development (Sea), (Doc Data Sheet only)

UNIVERSITIES AND COLLEGES

Australian Defence Force Academy
Library
Head of Aerospace and Mechanical Engineering
Deakin University, Serials Section (M list)), Deakin University Library, Geelong, 3217, (Research and Technical Reports only)
Senior Librarian, Hargrave Library, Monash University

OTHER ORGANISATIONS

NASA (Canberra)
AGPS

ABSTRACTING AND INFORMATION ORGANISATIONS

INSPEC: Acquisitions Section Institution of Electrical Engineers
Library, Chemical Abstracts Reference Service
Engineering Societies Library, US
American Society for Metals
Documents Librarian, The Center for Research Libraries, US

INFORMATION EXCHANGE AGREEMENT PARTNERS

Acquisitions Unit, Science Reference and Information Service, UK
Library - Exchange Desk, National Institute of Standards and Technology, US

ADDITIONAL DISTRIBUTION

Dr. Craig Tarver
Lawrence Livermore National Laboratory
L-282
University of California
PO BOX 808
Livermore, California 94550
USA

Dr. Paul Thibault
Combustion Dynamics Ltd.
No. 203, 132 4th Ave. S.E.
Medicine Hat, Alberta
CANADA T1A 8B5

Dr. Michael Cowperthwaite
SRI International - Poulter Laboratory
333 Ravenswood Avenue
Menlo Park, California 94025

Dr. David Kennedy
Mining Services Technology Centre
ICI Australia Operations Pty Ltd.
PO Box 196, George Booth Drive,
Kurri Kurri NSW 2327
Australia

Dr. Elaine Oran
Laboratory for Computational Physics and Fluid Dynamics
Naval Research Laboratory
Code 6404
4555 Overlook Ave. SW
Washington DC 20375-5000
USA

Dr. Jerry Forbes
Naval Surface Warfare Centre
10901 New Hampshire Ave.
Silver Spring, MD 20903-5640
USA

Total Number of Copies: 70

DEFENCE SCIENCE AND TECHNOLOGY ORGANISATION
DOCUMENT CONTROL DATA

1. PRIVACY MARKING/CAVEAT (OF DOCUMENT)

2. TITLE

Numerical Simulation Of Projectile Impact Experiments Using The Forest Fire Reaction Rate Model

3. SECURITY CLASSIFICATION (FOR UNCLASSIFIED REPORTS THAT ARE LIMITED RELEASE USE (L) NEXT TO DOCUMENT CLASSIFICATION)

Document	(U)
Title	(U)
Abstract	(U)

4. AUTHOR(S)

Rodney A. J. Borg & David A. Jones

5. CORPORATE AUTHOR

Aeronautical and Maritime Research Laboratory
PO Box 4331
Melbourne Vic 3001

6a. DSTO NUMBER	6b. AR NUMBER	6c. TYPE OF REPORT	7. DOCUMENT DATE
DSTO-TR-0325	AR-009-678	Technical Report	July 1996

8. FILE NUMBER	9. TASK NUMBER	10. TASK SPONSOR	11. NO. OF PAGES	12. NO. OF REFERENCES
510/207/0514	DST93/101	DSTO	22	20

13. DOWNGRADING/DELIMITING INSTRUCTIONS

—

14. RELEASE AUTHORITY

Chief, Weapons Systems Division

15. SECONDARY RELEASE STATEMENT OF THIS DOCUMENT

Approved for public release

OVERSEAS ENQUIRIES OUTSIDE STATED LIMITATIONS SHOULD BE REFERRED THROUGH DOCUMENT EXCHANGE CENTRE, DIS NETWORK OFFICE, DEPT OF DEFENCE, CAMPBELL PARK OFFICES, CANBERRA ACT 2600

16. DELIBERATE ANNOUNCEMENT

No limitations

17. CASUAL ANNOUNCEMENT Yes

18. DEFTEST DESCRIPTORS

Hydrocode Modelling Flux Corrected Transport Projectile Impact Forest Fire Reaction Rate Model Computational Modelling

19. ABSTRACT

We describe the development of a two-dimensional multimaterial reactive Eulerian hydrocode to model the detonation of condensed phase explosives, and use the code to model the projectile impact initiation of explosives. The code solves the Euler equations for the conservation of mass, momentum, and energy for an inviscid, compressible fluid using the Flux Corrected Transport algorithm. The condensed phase materials are modelled using a Mie-Gruneisen equation of state, while the Becker-Kistiakowsky-Wilson equation of state is used to describe the gaseous detonation products. The Forest Fire reaction rate model is used to describe the rate of energy release from the explosive, and a modified Young's algorithm is used to maintain a sharp interface between different materials on the computational mesh. The code was used to simulate the impact of a cylindrical steel projectile against Composition B explosive, and the threshold velocity for the onset of detonation was found to be dependent on the diameter of the projectile. Our computed results are in good agreement with experimental values, as well as with results obtained from Mader's 2DE reactive hydrocode. The work described here will provide the ADF with an improved methodology to assess bullet/fragment hazards, and assist in the development of an Insensitive Munitions capability.